(This is a sample cover image for this issue. The actual cover is not yet available at this time.)

Journal of Hydro-environment Research 21 (2018) 29–42

Contents lists available at ScienceDirect

Journal of Hydro-environment Research

journal homepage: www.elsevier.com/locate/jher

Research papers

On the three-dimensional flow of a stable tangential vortex intake

S.N. Chan[a,b], Q.S. Qiao[a], Joseph H.W. Lee[a,*]

[a] Department of Civil and Environmental Engineering, The Hong Kong University of Science and Technology, Clear Water Bay, Hong Kong, China
[b] Institute for Advanced Study, The Hong Kong University of Science and Technology, Clear Water Bay, Hong Kong, China

ARTICLE INFO

Keywords:
Tangential vortex intake
Swirling flow
Energy dissipation
Air entrainment
Air-core
Numerical modeling
Volume-of-Fluid
Computational fluid dynamics
Stormwater management

ABSTRACT

Tangential vortex intakes are compact hydraulic structures commonly used in water supply, drainage and sewerage systems to convey water from high to low elevations efficiently. Tangential vortex intakes can be designed to ensure stable flows for all discharges, with high energy dissipation in the absence of significant air entrainment. However, due to the complex three-dimensional (3D) flow in the tangential vortex intake, current theoretical models are not sufficiently complete to interpret the flow process reliably. This paper presents a 3D computational fluid dynamics study of a steady tangential vortex intake flow using the Volume-of-Fluid method. For the first time, the CFD model predictions are validated against detailed point velocity measurements using laser doppler anemometry (LDA) for a wide range of inflow conditions. For a flow less than the free drainage discharge, the inflow does not interfere with the swirling flow in the drop shaft. The streamwise horizontal x-velocity at the channel-dropshaft junction varies linearly with vertical distance, while the vertical velocity follows a parabolic relation. For larger discharges the pressure and inflow velocity field is notably modified by the dropshaft swirling flow interacting with the inflow issued from the junction. While the swirling flow in the dropshaft is highly asymmetrical, it is found that the local tangential velocity can be well-approximated by a Rankine vortex – with solid rotation (forced vortex) behavior near the air core and a free vortex behavior in the main flow. In the free vortex region the vertical velocity is approximately constant in the radial direction. The predicted head-discharge relations, velocity field, pressure, and air core sizes are in excellent agreement with data. In particular the variation of air core size with flow rate is successfully predicted for the first time. The present study offers comprehensive insights of tangential vortex intake flow, and provides a basis for the hydraulic design of such vortex intake structures.

1. Introduction

Tangential vortex intakes are commonly used in water supply, drainage and sewerage systems. A tangential intake is a compact hydraulic structure which consists of an approach channel with horizontal bottom and rectangular cross section, a steep tapering channel, a junction, and a drop shaft. The inflow enters tangentially into the drop shaft via the tapering channel, and the flow swirls down the drop shaft. The strong centrifugal effect in the swirling flow results in a stable air core which allows any entrained air to escape. It is well accepted that the tangential intake is a compact design that possesses the hydraulic advantage of a stable flow with high energy dissipation in the absence of significant air entrainment. However, the three-dimensional (3D) vortex flow in the tangential vortex intake is complicated and current theoretical models are not sufficiently complete to interpret the flow process reliably.

Extensive experimental and theoretical investigations have revealed the complexity and subtlety of the tangential vortex intake flow since the 1940's. Binnie and Hookings (1948) presented an analytical approach for predicting the head-discharge relation of swirling flow with air core in a dropshaft with bell-mouthed entrance ('morning glory' spillway). Brooks and Blackmer (1962) performed a comprehensive experiment study of tangential intake model for San Diego Ocean Outfall. Jain (1984) first proposed a one-dimensional theoretical model based on uniform open-channel flow concepts to predict the depth-discharge relation and air core sizes of tangential intake. Yet the analytical approach does not account for the convergence of the approach channel, the interaction of the approaching flow with the swirling vortex flow, and the asymmetrical feature of swirling vortex flow. Zhao et al. (2006) proposed a similar one-dimensional (1D) model for predicting the hydraulic performance of tangential intake. Lee et al. (2005, 2006), carried out a hydraulic model study of tangential intake for a stormwater interception and transfer project in Hong Kong. They found that the hydraulic characteristics of tangential intake depends heavily

* Corresponding author.
E-mail address: jhwlee@ust.hk (J.H.W. Lee).

https://doi.org/10.1016/j.jher.2018.07.001
Received 26 February 2018; Received in revised form 15 May 2018; Accepted 19 July 2018
Available online 21 July 2018
1570-6443/

on its geometrical features. More importantly, they pointed out that the blocking effect by the swirling flow on the tapering channel outlet can cause unstable inflow in the tapering channel. Based on the experimental results of a series of hydraulic models and a 1D model assuming symmetrical free vortex flow, a stable design criterion for tangential intake was proposed (Yu and Lee, 2009). One important limitation of all the 1D models is the inability to predict the air core size accurately – with significant discrepancies between predictions and observations (e.g. Jain, 1984; Yu and Lee, 2009).

The velocity field of free-surface air core vortices induced by submerged vertical and horizontal intakes have been studied by Odgaard (1986) and Hite and Mih (1994) respectively. Confirmed by experiments, both studies proposed a Rankine-type of combined vortex model for the axisymmetrical forced vortex and free vortex in the inner and outer regions respectively. The relation of these analytical solutions to the complex 3D asymmetric tangential vortex flow is not clear; there are also hitherto no basic velocity field measurements. More recently, we have carried out the first set of detailed velocity and air core size measurements on the flow structure of a stable tangential intake vortex flow (Qiao et al., 2013).

With the development of computational modeling techniques and advancement in computation power, attempts have been made to tackle the air-water flow in vortex intake problems using 3D Computational Fluid Dynamics (CFD) models with the Volume-of-Fluid (VOF) method. The interface between the water and air can be located and tracked when it moves through the computational domain. Recently Plant and Crawford (2016) has reported the use of 3D CFD model on the design of a tangential vortex intake for the Thames Tideway Tunnel, London, UK in conjunction with an experimental study. The CFD model has been compared with measured head-discharge relation, however there has been hitherto no detailed validation of CFD model prediction with velocity measurements. This paper presents a 3D CFD modeling on a stable tangential intake vortex flow. For the first time, the numerical model results are validated against detailed flow profile, flow velocity and air core measurements on a tangential vortex intake. In this paper, the experimental set-up and measurement techniques are first presented, followed by the details of the CFD model. The numerical model results are compared with experimental measurements and discussed.

2. Experimental set-up

The flow characteristics of a tangential vortex intake is mainly determined by the following design parameters: e = junction width, B = approach channel width, D = drop shaft diameter, β = bottom slope of tapering section, and θ = tapering angle of width of tapering section. For the laboratory model used in this study, $D = 0.124$ m, $e = 0.031$ m, $B = 0.124$ m, $\beta = 13°$, and $\theta = 24°$ (Fig. 1). The model parameters fulfill the stable design criteria established by Yu and Lee (2009) where the free drainage discharge of the tangential vortex intake Q_f should be greater than the discharge capacity Q_c, where Q_f and Q_c are defined respectively

$$Q_f = \left(\tan\beta\frac{\pi D}{1-e/D}\right)^{3/2}\sqrt{g}\,e\cos^2\beta \tag{1}$$

$$Q_c = \frac{\sqrt{g}\,e(2z/3)^{3/2}}{(\cos^{2/3}\beta-(e/B)^{2/3})^{3/2}} \tag{2}$$

where $z = (B-e)\frac{\tan\beta}{\tan\theta} = 0.048$ m is the drop in elevation between the approach flow channel and the junction to dropshaft. The free drainage discharge Q_f and the discharge capacity Q_c predicted under the design geometry are 3.81 L/s and 1.24 L/s respectively. For a stable tangential vortex intake ($Q_f > Q_c$), three regimes of flow occurs (Yu and Lee, 2009): (i) when $Q < Q_c$, the flow control is at the end of the approach

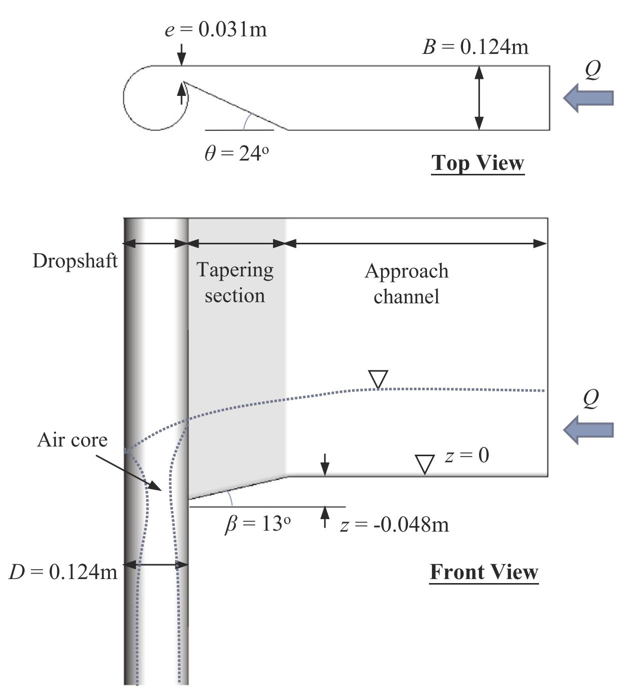

Fig. 1. Geometry of the laboratory model of stable tangential vortex intake.

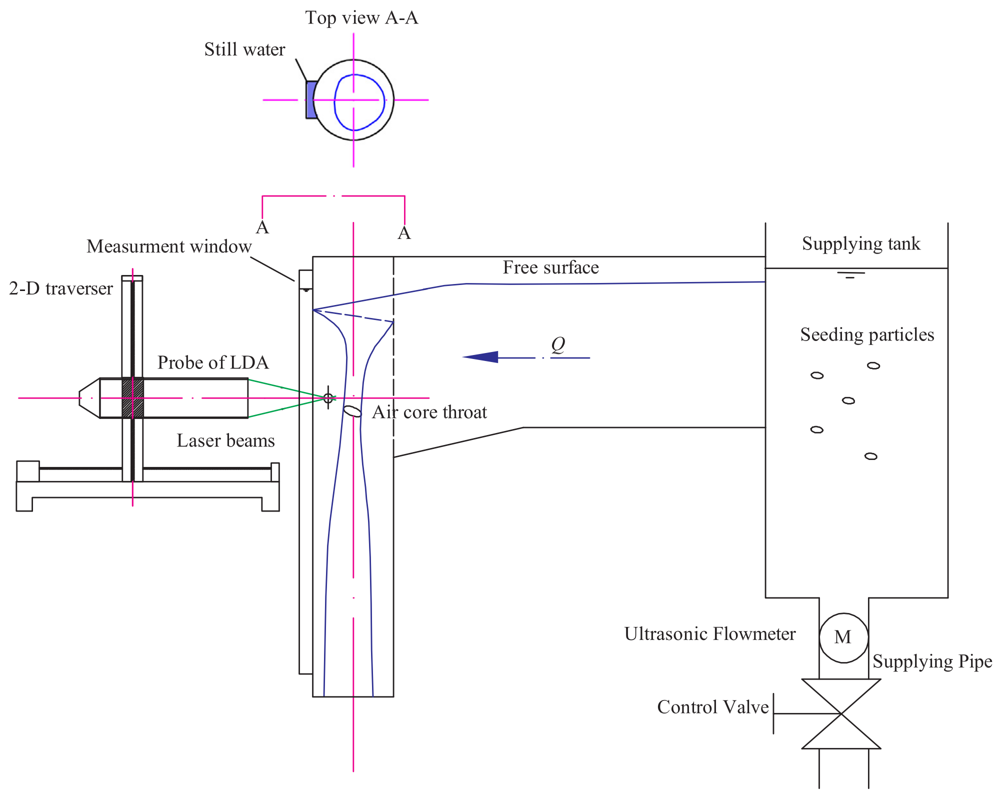

(a)

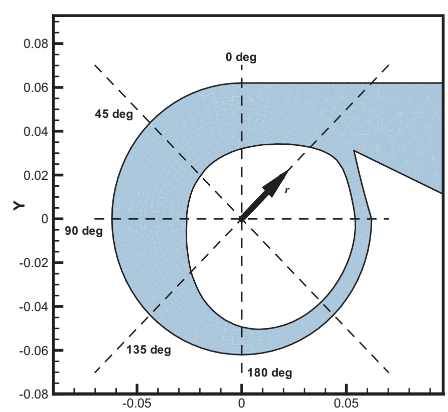

(b)

Fig. 2. (a) Experimental set-up for Laser Doppler Anemometry (LDA) flow measurement in the dropshaft, (b) Transects of swirling flow measurement in the dropshaft.

flow channel where critical flow occurs along the entire horizontal channel; (ii) when $Q_c \leqslant Q < Q_f$, the flow control shifts to the junction between the tapering section and the dropshaft; the flow becomes subcritical in the entire tapering channel, and the top surface of the vortex flow after a 360° turn is below the bottom of the junction, thus not affecting the critical flow at the junction; (iii) when $Q \geqslant Q_f$, the vortex flow interacts with the inflow at the junction, resulting in backing up of the flow at the tapering channel and approach channel.

The physical model of stable tangential intake is fabricated from Perspex. A steady discharge Q through the model is generated by a

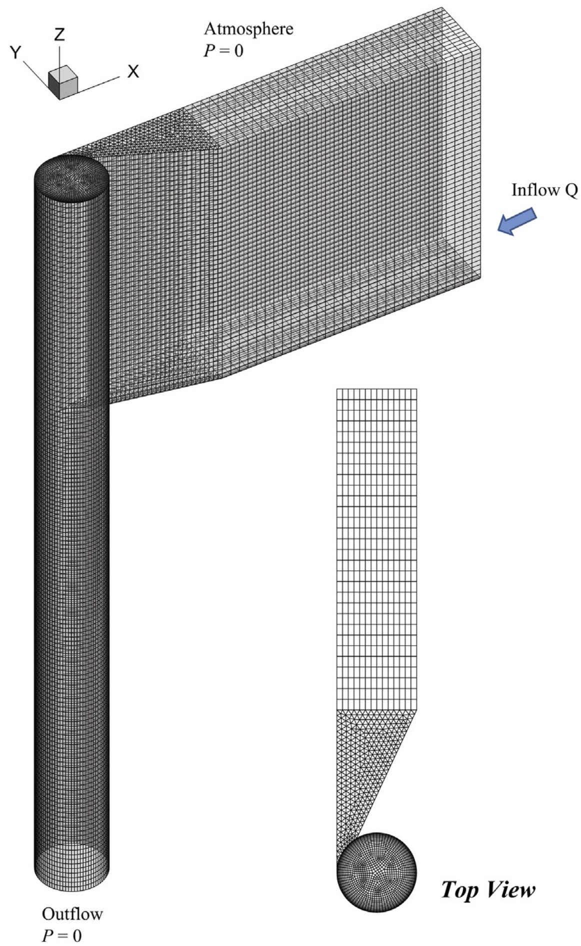

Fig. 3. The computational mesh of a stable tangential vortex intake design.

water recirculating system feeding into a header tank for the vortex intake model. All experiments are carried out at steady flow for a range of flow conditions varying from $Q = 1.0$ L/s to 10.0 L/s, and the Reynolds number of the approach channel flow is of order of 10^5; turbulent flow conditions are attained in the model.

Based on experimental observations (Yu and Lee, 2009), the flow process in the model can be divided into two regions – the inflow bounded by the straight walls of the tapering channel, and the swirling flow bounded by the circular wall of the drop shaft. In the approach channel and the junction between tapering channel and the dropshaft, the flow depths are measured with a point gauge. The thickness of the vortex flow (and air core) in the dropshaft is determined at different elevations by a specially designed eight-leg ruler (Yu and Lee, 2009). This air core measurement device consists of eight tiny metal rods drilled into a 5-mm thick transparent perspex disk of 15 mm diameter, at azimuthal intervals of 45° (Yu and Lee, 2009). The velocity field is measured by laser doppler anemometry using a two-component DANTECH LDA (Dantec Dynamics, 2006). In the tapering channel, the 3D inflow velocity field is measured in a Cartesian coordinate system, and the streamwise horizontal velocity u, the transverse velocity v perpendicular to the straight vertical boundary wall, and the vertical velocity w are measured. In the drop shaft the tangential and vertical velocity components of the swirling flow are measured. Refraction of light by the curved surface wall of the dropshaft was avoided by a specially designed water-filled measurement perspex panel (window) mounted to the external wall of the dropshaft as shown in Fig. 2a). The tangential velocity u_θ, radial velocity u_r and vertical velocity w in the dropshaft are measured for five transects (0°, 45°, 90°, 135° and 180°) shown in Fig. 2b. Pressure measurements are also made by a set of piezometers installed at several elevations on the vertical wall of the tapering section as well as the dropshaft. Details of experimental set-up and measurement techniques can be found in Yu and Lee (2009) and Qiao et al. (2013).

3. Computational fluid dynamics model

3.1. Governing equations

The Volume-of-Fluid (VOF) model (Hirt and Nichols, 1981) predicts two immiscible fluids (water and air) by solving a single set of momentum equations and tracking the volume fraction of each of the fluids throughout the domain. The tracking of the interface between the phases is accomplished by the solution of a continuity equation for the volume fraction of one of the phases. For the water phase, this equation has the following form:

$$\frac{\partial}{\partial t}(\alpha_w \rho_w) + \nabla\cdot(\alpha_w \rho_w \mathbf{U}) = 0 \tag{3}$$

where α_w is the volume fraction for the water phase. The volume fraction for the air phase α_a will be computed based on the constraint of $\alpha_a + \alpha_w = 1$. In a two-phase system, the air-water mixture density ρ and dynamic molecular viscosity μ in each cell is given by

$$\rho = \alpha_w \rho_w + (1-\alpha_w)\rho_a \tag{4}$$

$$\mu = \alpha_w \mu_w + (1-\alpha_w)\mu_a \tag{5}$$

where the densities of air and water are treated as constant of $\rho_a = 1.225\ \mathrm{kg/m^3}$ and $\rho_w = 998.2\ \mathrm{kg/m^3}$ respectively; the dynamic molecular viscosity of air and water are $\mu_a = 1.8 \times 10^{-5}$ kg/m/s and $\mu_w = 1.0 \times 10^{-3}$ kg/m/s respectively.

A single momentum equation is solved throughout the domain, and the resulting velocity field $\mathbf{U} = (u, v, w)$ is shared among the phases. The momentum equation below, is dependent on the volume fractions of all phases through the properties ρ and μ_t.

$$\frac{\partial}{\partial t}(\rho \mathbf{U}) + \nabla\cdot(\rho \mathbf{U}\mathbf{U}) = -\nabla P + \nabla\cdot[(\mu + \mu_t)(\nabla \mathbf{U} + \nabla \mathbf{U}^{\mathrm{T}})] + \rho \mathbf{g} \tag{6}$$

where P is the pressure; $\mathbf{g} = (0, 0, -9.81)\ \mathrm{m/s^2}$ is the gravitational acceleration. The turbulent dynamic viscosity μ_t for air-water mixture is determined using the two-equation standard $k-\varepsilon$ turbulence model, where k is the turbulent kinetic energy and ε is its dissipation rate. The continuity equation of both air and water phases is used to determine the pressure P through the PISO algorithm for velocity-pressure correction:

$$\frac{\partial \rho}{\partial t} + \nabla\cdot(\rho \mathbf{U}) = 0 \tag{7}$$

The governing Eqs. (3), (6), (7), and the k and ε equations of the turbulence model are solved numerically using the finite volume method in the commercial CFD code of ANSYS FLUENT 15 (ANSYS Inc.,

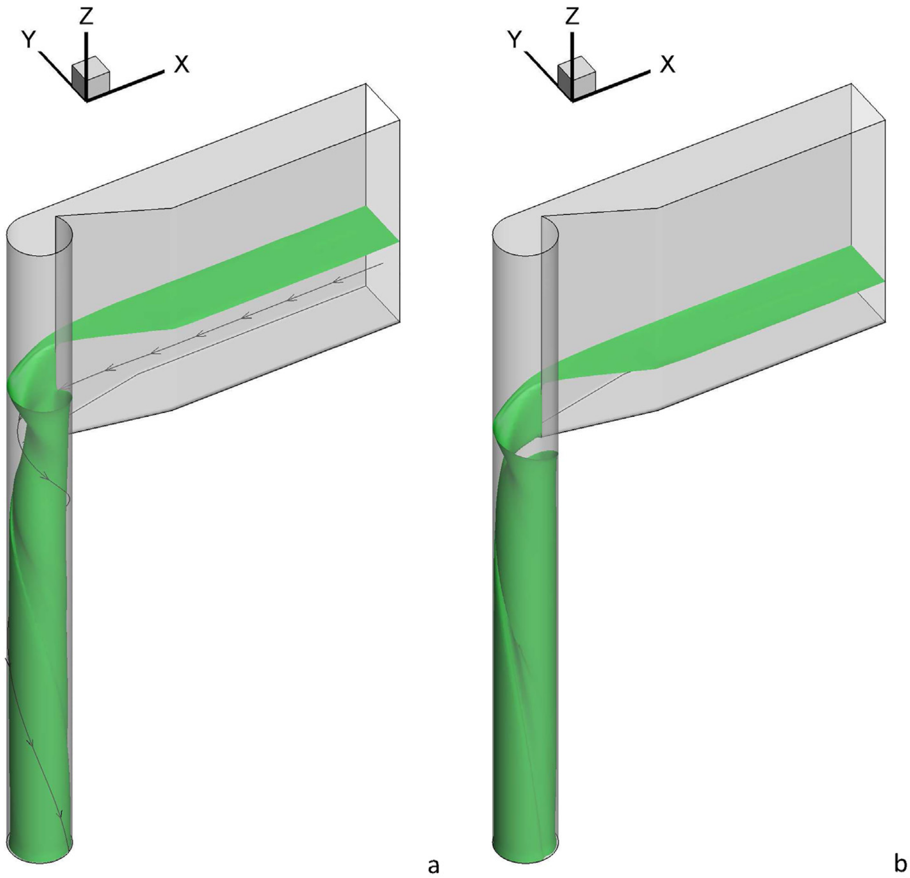

Fig. 4. Predicted free surface profile (as 50% air concentration) for (a) 8 L/s, (b) 4 L/s. A pathline from computed velocity is shown in (a) to illustrate the swirling flow in the dropshaft.

2013). A second order upwind advection scheme is used for momentum and density, while a first order upwind advection scheme is used for k and ε. The volume fraction equation (Eq. (3)) is spatially discretized using the Modified High Resolution Interface Capturing (HRIC) Scheme in FLUENT, which provides improved accuracy for VOF calculations for the implicit solution of volume fraction (with less stringent requirement for stability than using explicit solver). The under-relaxation factors for the iterative solver are 0.5 for pressure and momentum, 0.2 for volume fraction, 0.8 for k and ε, and 1.0 for density and turbulent viscosity. Convergence for each time step is declared when the normalized residual is less than 10^{-4} for all variables.

3.2. Model grid, boundary and initial conditions

The model grid of the tangential vortex intake is developed according to the experimental design. An unstructured boundary-fitted model grid is used for numerical simulation (Fig. 3). The computational mesh has 278,650 grid cells with hexahedral cells for the approach channel and dropshaft, and triangular-prismatic cells for the tapering channel. Mesh refinement is made to the region close to the dropshaft wall to resolve the swirling flow attached to the wall (Fig. 3). The minimum grid size near the dropshaft wall region are ~ 1 mm. Mesh convergence is tested using a coarser mesh with 80,600 cells, showing less than 5% difference to the predicted velocity profiles and air core sizes.

The computational model has three open boundaries – the inflow, the outflow for vortex dropshaft and the top atmospheric boundary. The upstream inlet of the approach channel is prescribed with the total water flow rate and a head discharge relation at the inlet of the model measured experimentally. The upper boundary of the CFD model is prescribed with zero gauge pressure/atmospheric pressure. The outlets of the vortex dropshaft are prescribed with zero gauge pressure. A roughness height of 0.01 mm is prescribed for all wall boundaries.

Numerical predictions are carried out for the six flow rates of $Q = 1$, 2, 4, 6, 8 and 10 L/s, corresponding to the cases in the experimental study. The model is run with an initially dry condition. The supercritical flow in the approach channel and the vortex intake develops from the inlet. A time step of 0.001 s is used for the simulation and typically about 10–15 s of flow simulation are required for the vortex flow to be developed into steady state. The run time for 10 s of flow is $\approx$40 h on a Dell workstation with an Intel i7-6700 3.4 GHz CPU with quad-core parallel computation.

4. Results and discussions

4.1. Flow profile and head-discharge relation

The predicted 3D flow (free surface) profile is shown in Fig. 4. It is observed that the free surface in the approach channel and tapered channel of this tangential vortex design is relatively steady without any

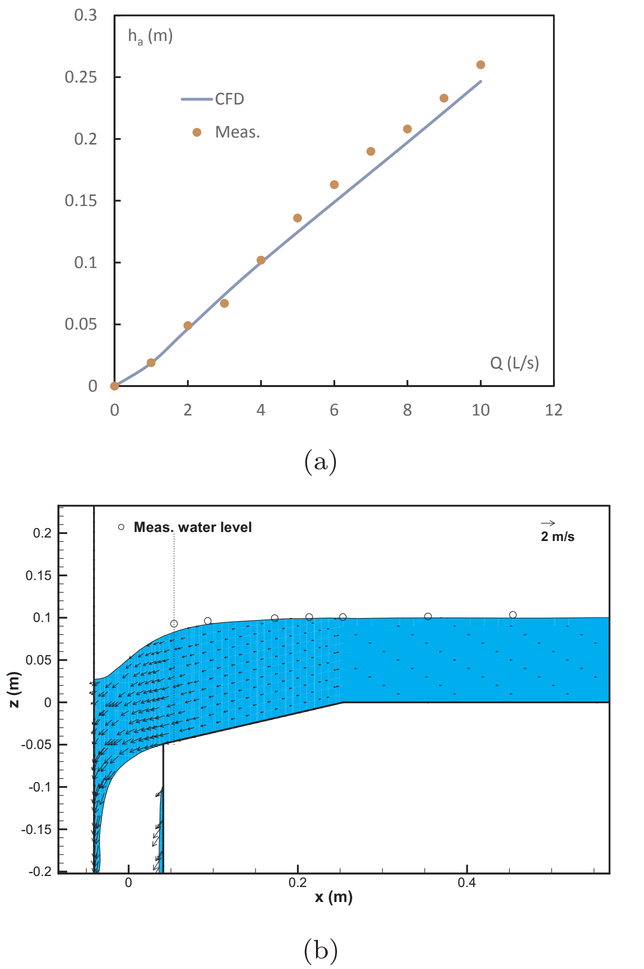

Fig. 5. (a) Measured and predicted head-discharge relation, (b) measured and predicted flow depth and flow field at the tapering and approach channel ($Q = 4$ L/s). Free surface defined as 50% air concentration.

hydraulic jump, instability or shock waves for both flows (8 L/s and 4 L/s). The model prediction clearly illustrates the characteristics of a stable tangential vortex design. A pathline initiated from the inlet is shown in Fig. 4a for the high flow situation ($Q = 8$ L/s $> Q_f$). The pathline is straight in the approach and tapered channel and swirls down along the periphery of the dropshaft. The flow after a 360° turn impacts on the lower part of the flow from the approach channel slot. For the low flow ($Q = 4$ L/s $\approx Q_f$, Fig. 4b), the swirling flow starts at the slot and swirls down the dropshaft, after a 360° turn the free surface is just below the bottom of the inflow slot and does not interact with the inflow.

Fig. 5a shows the measured flow depth under varying discharge Q, and the prediction with the CFD model (defined as 50% air concentration). It is seen that the water depth at the approach channel h_a approximately varies linearly with Q for large discharge, and the predicted depth agrees well with measurement. Fig. 5b shows the flow depth and flow field at a vertical transect of the tapering channel and the junction for $Q = 4.0$ L/s. The surface level is almost flat compared to the bottom slope of the tapering channel, indicating that the flow control has been shifted to the junction ($Q > Q_c$) and resulting in a subcritical flow in the tapering channel. It can be seen that the flow accelerates from the approach channel to the junction, due to the narrowing and sloping of the tapering channel.

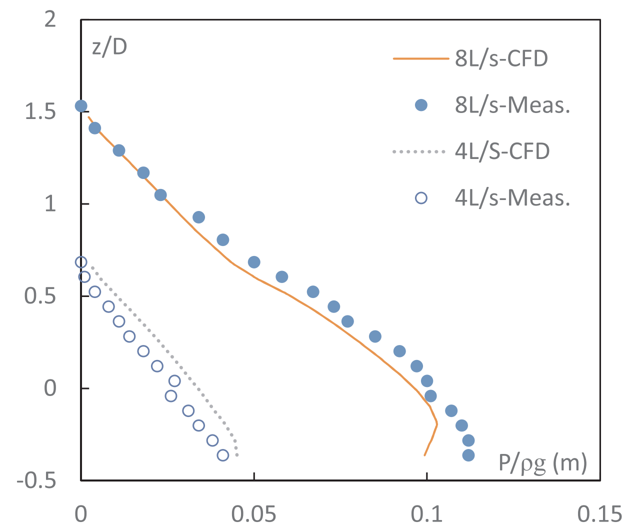

Fig. 6. Predicted static pressure distribution at junction.

4.2. Pressure and flow field at the tapering channel-dropshaft junction

Fig. 6 shows the measured and predicted static pressure head at $x \approx 0.0$ m for $Q = 4.0$ and 8.0 L/s. It is seen that the predicted static pressure head compares well with the measured. For this comparison the measured pressure head $P/\rho g$ refers to the static pressure head inferred from the direct 3D velocity measurements, given by $P/\rho g = H - U^2/2g - z$, where $H = U_a^2/2g + h_a$ is the total energy head. U_a and h_a are the measured velocity and depth of the uniform approach flow, $U^2/2g$ ($U^2 = U_x^2 + U_y^2 + U_z^2$) is the velocity head and z is the elevation head. For the stable vortex intake design, experiments have shown that energy conservation can be assumed throughout the approach and tapering channels. For $Q = 4.0$ L/s it is seen that the pressure variation is approximatley linear but much less the hydrostatic pressure – for example at the junction the static pressure head is 0.042 m vs 0.13 m respectively. It can be shown that the significant vertical velocities resulted in the reduction of the pressure head below the hydrostatic value throughout the depth. Similarly, for $Q = 8.0$ L/s, the pressure variation with depth is linear for the top half layer of flow ($0.75 < z/D < 1.5$), but becomes non-linear in the bottom half ($0 < z/D < 0.75$) possibly due to the backing up by the circulating flow in the dropshaft. Overall the pressure is much less than the hydrostatic

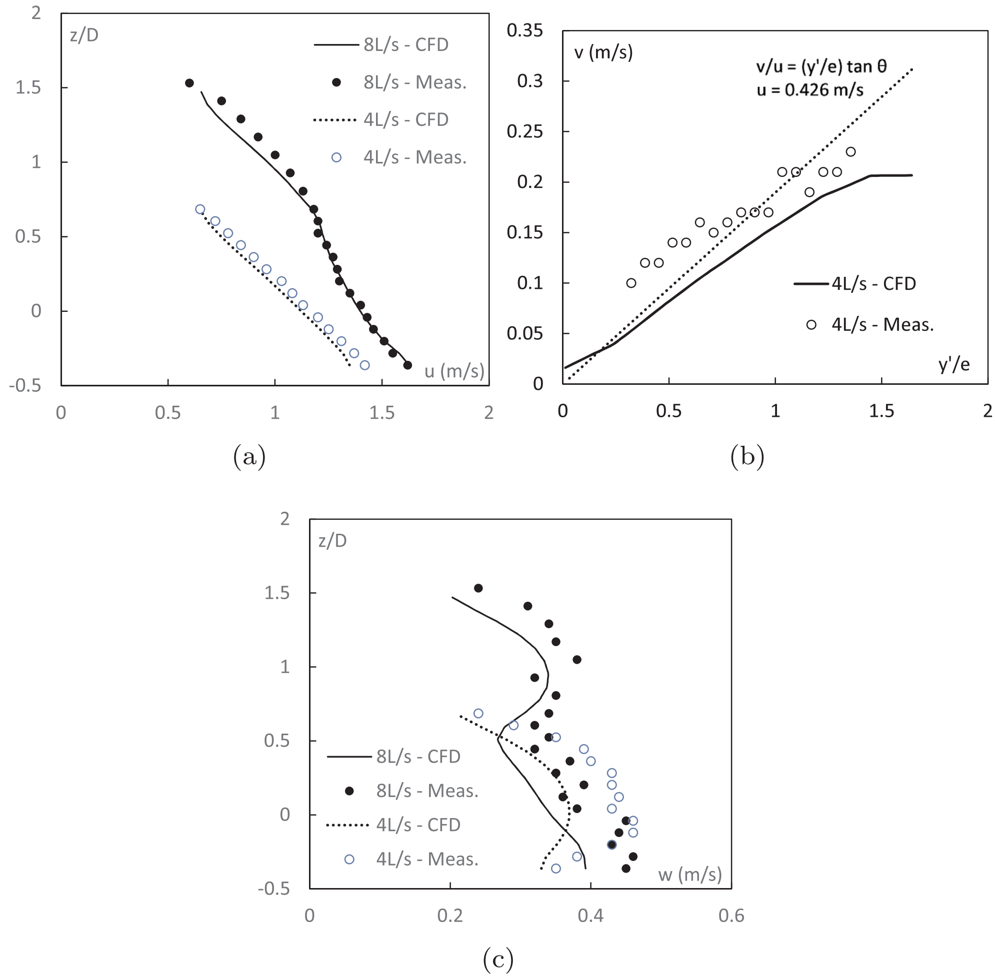

Fig. 7. Predicted and measured (a) horitzontal x-velocity u at tapering channel – dropshaft junction; (b) transverse velocity v at 0.045 m upstream of junction ($z = 0.05$ m). y' is measured from the outer (straight) side of tapering channel; (c) vertical velocity w at tapering channel – dropshaft junction.

pressure (e.g. 0.11 m vs 0.24 m near the bottom).

The turbulent-mean Cartesian velocities u, v and w are measured at the outlet of the tapered section. Fig. 7a shows the comparison of predicted and measured vertical variation of x-velocity u for $Q = 4.0$ and 8.0 L/s at the junction. It is observed that near the junction u varies approximately linearly in the vertical direction, and the transverse gradient of the x-velocity $\frac{\partial u}{\partial y}$ is relatively small for $Q = 4.0$ L/s. Note that the free drainage condition holds in this case. The linear variation of x-velocity is confirmed experimentally for $Q \leqslant 4.0$ L/s (Qiao et al., 2013). For larger flow the linear velocity profile of u is notably modified close to the bottom of the inlet channel by the circulating flow in the drop-shaft. It is also observed that the transverse variation of y-velocity over the narrow junction slot can be approximated by a linear transverse variation $v = u\tan\theta\ (y/e)$ (Fig. 7b).

Fig. 7c shows the measured vertical velocity profile w at $x = 0.0$ and $y = 0.009$ m for $Q = 4.0$ and 8.0 L/s. For the free drainage condition ($Q \leqslant 4.0$ L/s), it is found that the measured vertical velocity w has an approximately parabolic profile, with the maximum vertical velocity at mid-depth. In the upstream region of the junction, similar parabolic distributions of w have also been observed under these two discharges (not shown). The parabolic variation of the vertical velocity is a direct consequence of the linear transverse variation of the y-velocity based on the continuity equation. For $Q = 8.0$ L/s, the velocity profiles w is affected by the drop shaft flow, and deviate from the parabolic shapes at the bottom of the flow ($0 < z/D < 0.5$).

4.3. Air core

Fig. 8 shows the predicted swirling flow in the drop shaft for four representative discharges, Q = 2–10 L/s. The inflow from the tapering channel enters the dropshaft as a slot jet. It is seen that the air core is significantly asymmetrical about the axis of the drop shaft; the flow thickness is largest near the junction entry and decreases gradually as it swirls around the circumference. For the smaller flows, $Q \leqslant 4.0$, the thickness of the flow layer is almost zero in the region around $\theta = 270°$ L/s (Fig. 8a and b). Fig. 9a shows the variation of normalized

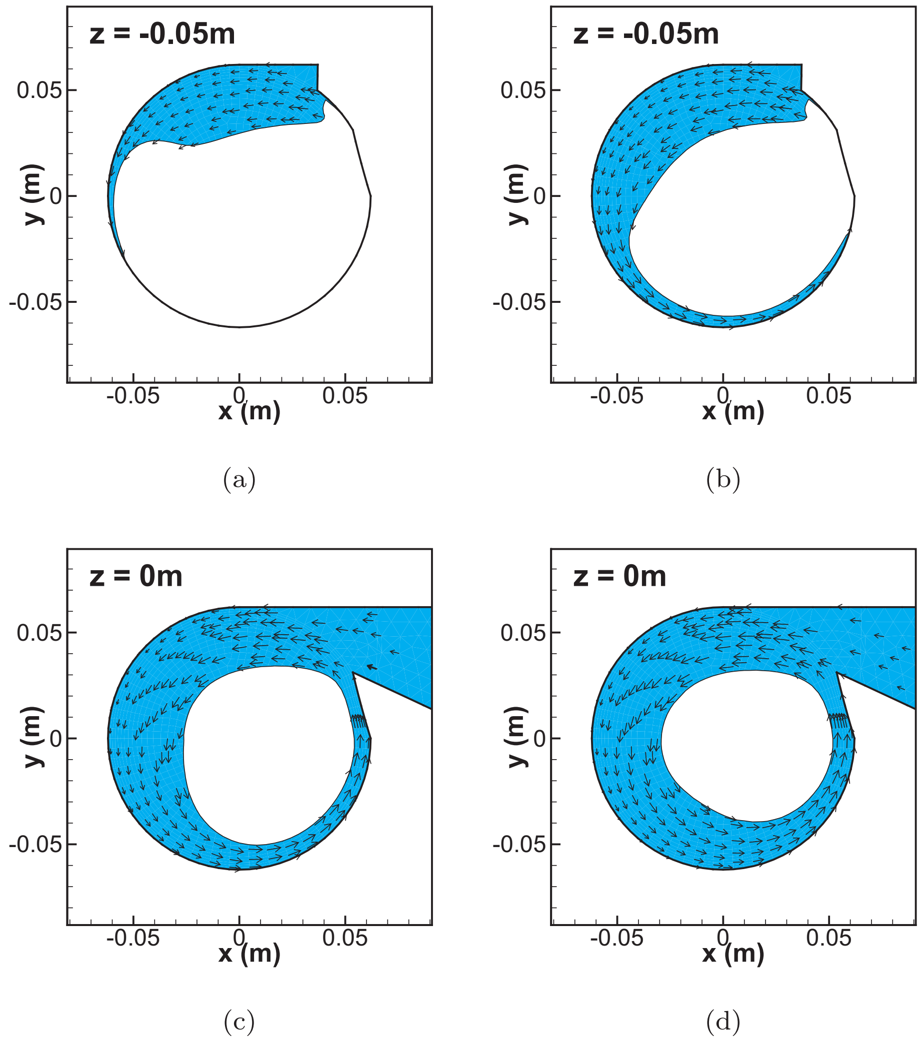

Fig. 8. Predicted shapes of the minimum air core: (a) 2 L/s (z = −0.05 m), (b) 4 L/s (z = −0.05 m), (c) 8 L/s (z = 0 m), (d) 10 L/s (z = 0 m). Free surface defined as 50% air concentration.

air core area λ (ratio of air core area to the dropshaft cross-sectional area) with the level z. There obviously exists a minimum λ_m at certain level z – which increases with increasing Q. The location of minimum air core (the throat) for $Q = 8$ and 10 L/s is at $z = 0$ to $z = -0.5$ m; while for the smaller flows ($Q = 2$ and 4 L/s) the throat is located at around $z = -0.5$ m. The general vertical variation of the air core area is well captured by the numerical predictions. Fig. 9b) shows the predicted minimum λ_m as a function of discharge. It is seen that the predicted air core area ratio is in excellent agreement with data, showing a decreasing trend of minimum air core size with increasing discharge. The model prediction is slightly higher than that of the measurement for larger flows, possibly due to the error induced by the measurement method using a eight-legged ruler which results in some blockage of flow (Qiao et al., 2013). The prediction of air core area (an important vortex intake design parameter) is significantly better than what can be achieved with a 1D model that assumes symmetry (e.g. Yu and Lee, 2009).

4.4. Flow field at the dropshaft

The comparison of predicted and measured tangential and vertical velocities along different angular transects and elevations in the dropshaft for $Q = 8$ L/s is shown in Fig. 10. The predicted velocity distribution at a level around the throat (z = −0.04 m) compares well with LDA measurement. It can be seen that the tangential velocity u_θ increases linearly from near the air core in the center to a maximum at $r_m = 0.04$ m and then falls off with radius resembling a free vortex. A thin boundary layer of sharp velocity gradient close to the dropshaft

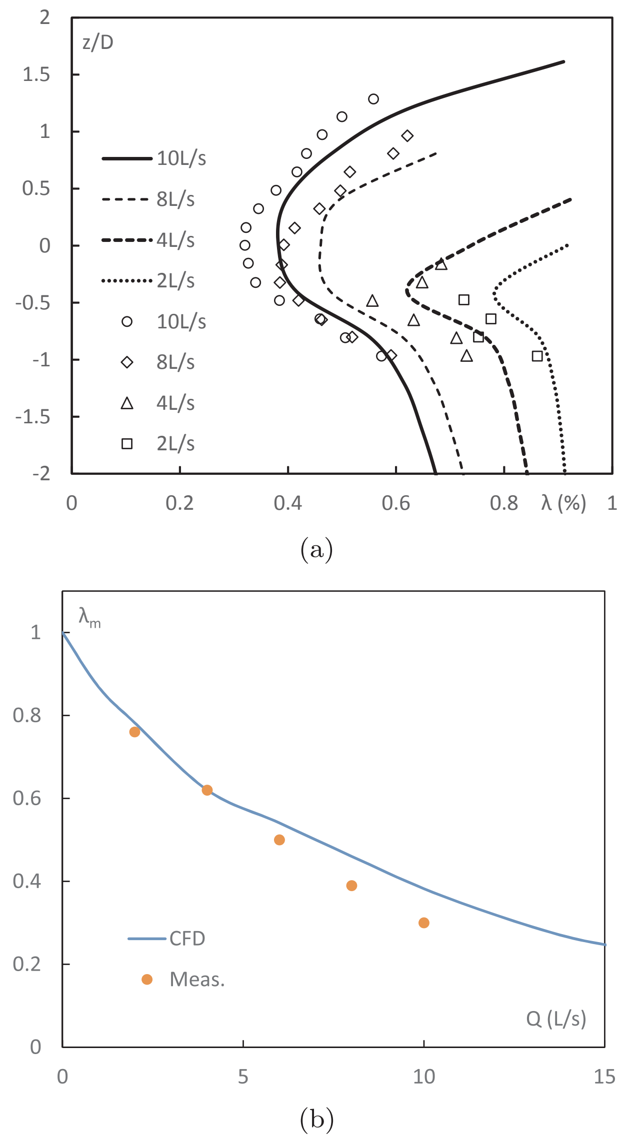

Fig. 9. (a) Air core area ratio vs elevation along the dropshaft (lines: CFD, symbols: measurement); (b) Predicted and measured minimum air core ratio vs flow rate.

wall at $r = 0.062$ m can be noted. The reduced velocity near the center is due to viscous dissipation and the increase in downward vertical velocity. The tangential velocity increase with radius near the air core is suggestive of solid body rotation (forced vortex) behavior. It is noted that the free vortex region is characterized by approximately constant vertical velocities of around 1.2–1.4 m/s; on the other hand, in the central core of the swirling flow, the vertical velocity increases. The pressure and velocity measurements suggest that the energy is conserved in the outer free vortex region, but there is minor energy dissipation in the central vortex core (not shown). The flow thicknesses are different at the four angular positions, with largest thickness at 90° (about 0.032 m) and the smallest thickness at 180° (about 0.012 m). The vortex flow thickness is further reduced at a lower elevation $z = -0.12$ m (Fig. 11) to about 0.02 m due to the increase in flow velocity under gravity to about 2 m/s. As the flow swirls down, the vertical velocity increases and the flow thickness decreases; the flow becomes more symmetrical. At $z = -0.12$ m, the flow thickness at 90° and 135° angular transects are similar, but slightly greater at the 135° transect (around 0.017 m and 0.018 m respectively). The radial variation of tangential and vertical velocity is similar to that at the throat, with a larger vertical velocity of around 2 m/s.

Fig. 12 shows the comparison of predicted and measured velocity

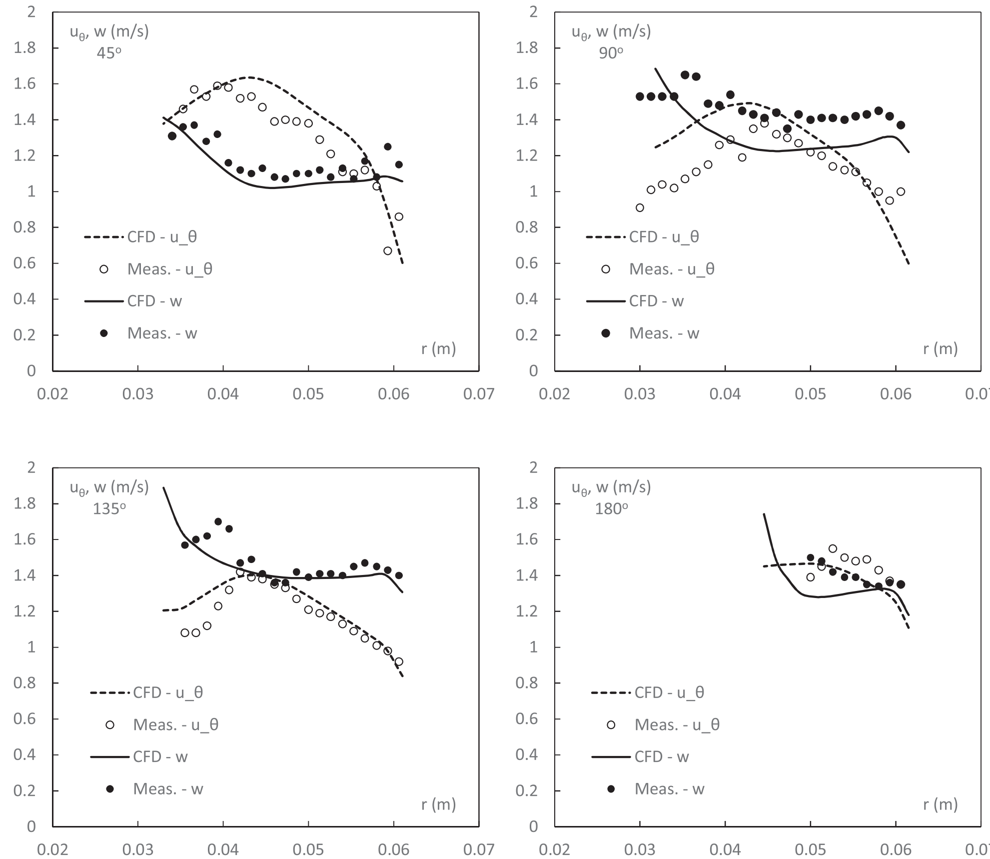

Fig. 10. Predicted and measured tangential velocity u_θ and vertical velocity w along 4 azimuthal transects (45°, 90°, 135°, 180°) in the dropshaft for $Q = 8$ L/s at $z = -0.04$ m. The azimuthal locations are shown in Fig. 2b.

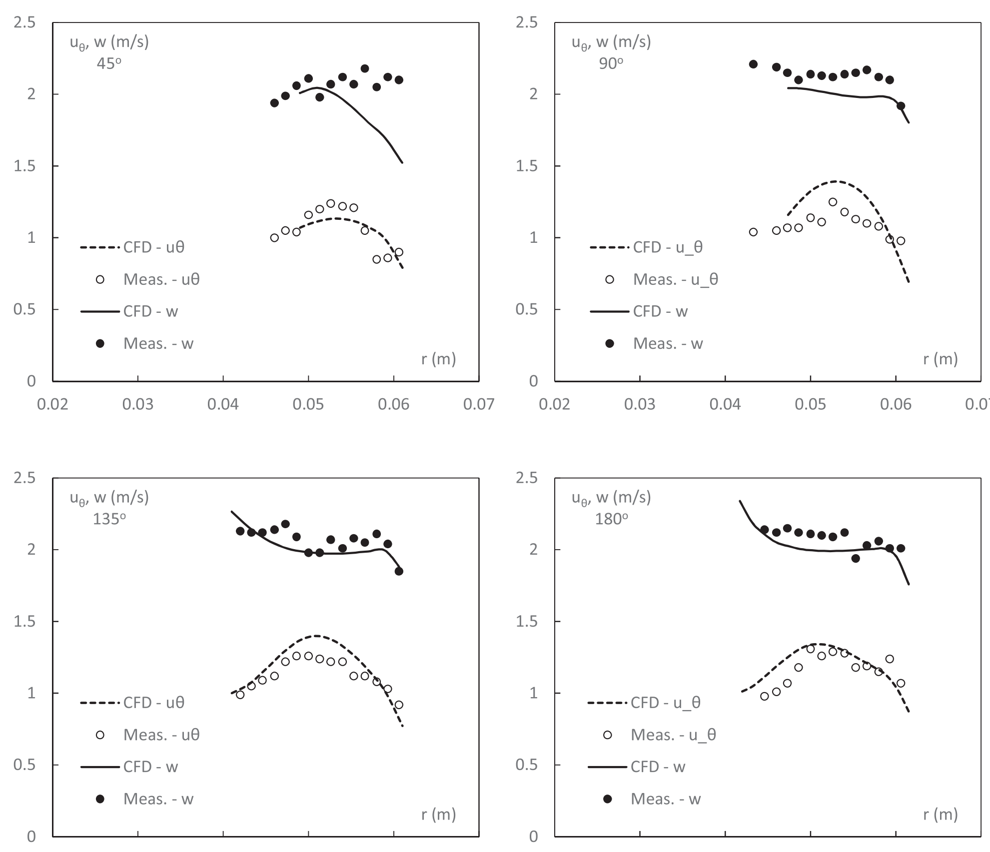

Fig. 11. Predicted and measured tangential velocity u_θ and vertical velocity w along 4 azimuthal transects (45°, 90°, 135°, 180°) in the dropshaft for $Q = 8$ L/s at $z = -0.12$ m. The azimuthal locations are shown in Fig. 2b.

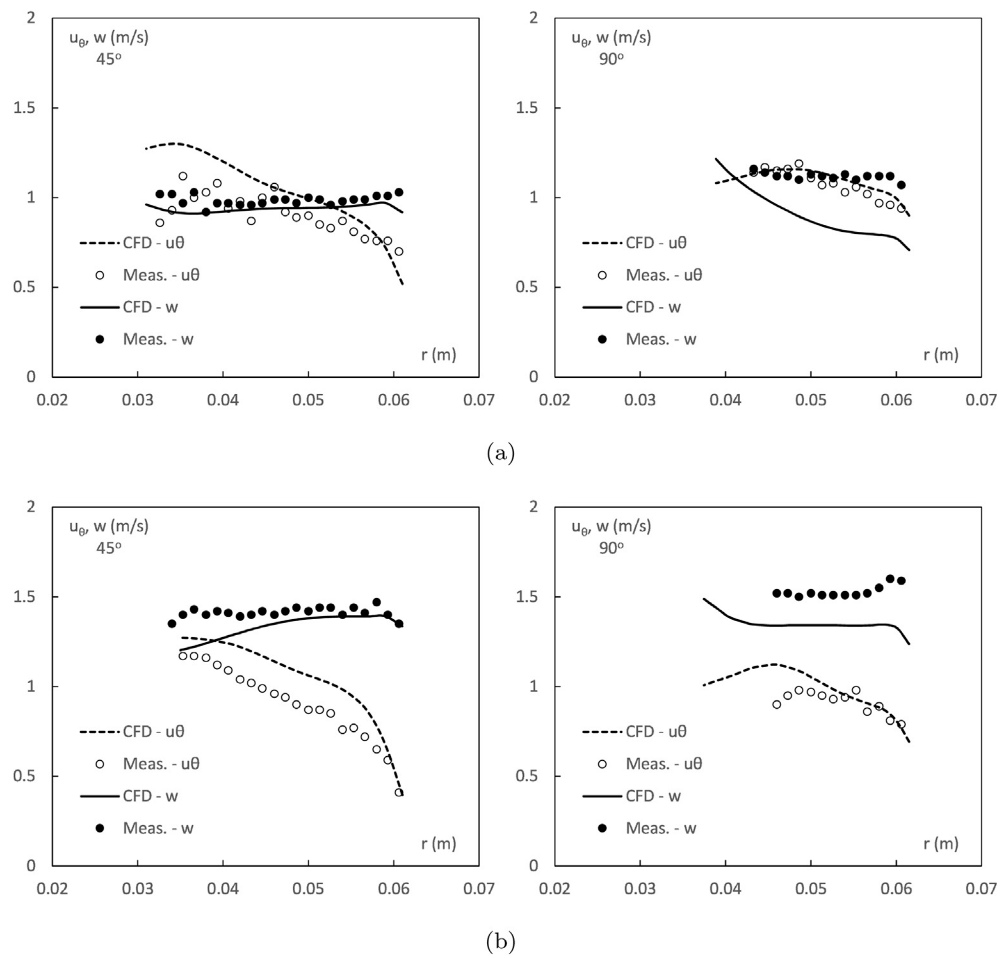

Fig. 12. Predicted and measured tangential velocity u_θ and vertical velocity w along 2 azimuthal transects (45°, 90°) in the dropshaft for $Q = 4$ L/s. (a) $z = -0.04$ m, (b) $z = -0.08$ m. The azimuthal locations are shown in Fig. 2b.

for $Q = 4$ L/s. Due to the small thickness of flow at 135° and 180°, only the results at 45° and 90° are shown. The smaller flow rate is accompanied by a reduction in both tangential and vertical velocity. Although model predictions can differ from observations by up to 20–30%, the overall velocity trend and characteristics are well predicted by the model and similar to that for $Q = 8$ L/s. The average error for the tangential velocity u_θ is about 10% while that for the vertical velocity w about 7%. It should be noted that for smaller flow rates or at a lower elevation in the dropshaft, the thin swirling flow layer may not be sufficiently resolved by the numerical model grid (radial grid size of about 1 mm) and may be affected by wall friction and surface tension. The overall error of the velocity measurement in the complex swirling flow can be estimated to be around 10%.

To examine the flow behavior in more detail, Fig. 13a and b show respectively the z-component of the vorticity and turbulent kinetic energy (TKE) fields at the level of the throat for $Q = 4$ L/s and 8 L/s respectively. It is seen that the vorticity and areas of significant TKE are confined to near the air core and the dropshaft wall, with a region of inviscid flow in the main of the swirling flow. This can be clearly seen if the local circulation defined by $\Gamma = u_\theta \times r$ is plotted against radius for different azimuthal positions (Figs. 14 and 15). For the tangential vortex, the vortex circulation induced by the approach flow at the junction is given by $\Gamma_a = u_x(D/2{-}e/2)$, where u_x = average horizontal inflow velocity at tapering channel-dropshaft junction. For Q = 8 L/s a free vortex region with constant local circulation is clearly evident (Fig. 14), with $\Gamma \approx \Gamma_a = 0.061$ m^2/s. The increase of circulation in the forced vortex region near the air core is also well predicted. Similar behavior is observed for $Q = 4$ L/s (Fig. 15). It is interesting to note that – at least to first order – the swirling flow field can be interpreted using a robust Rankine type vortex model developed for air-core vortices induced by submerged intakes (Odgaard, 1986; Hite and Mih, 1994).

5. Conclusions

The three-dimensional velocity field of a tangential vortex intake is studied experimentally and numerically for the first time. A 3D CFD

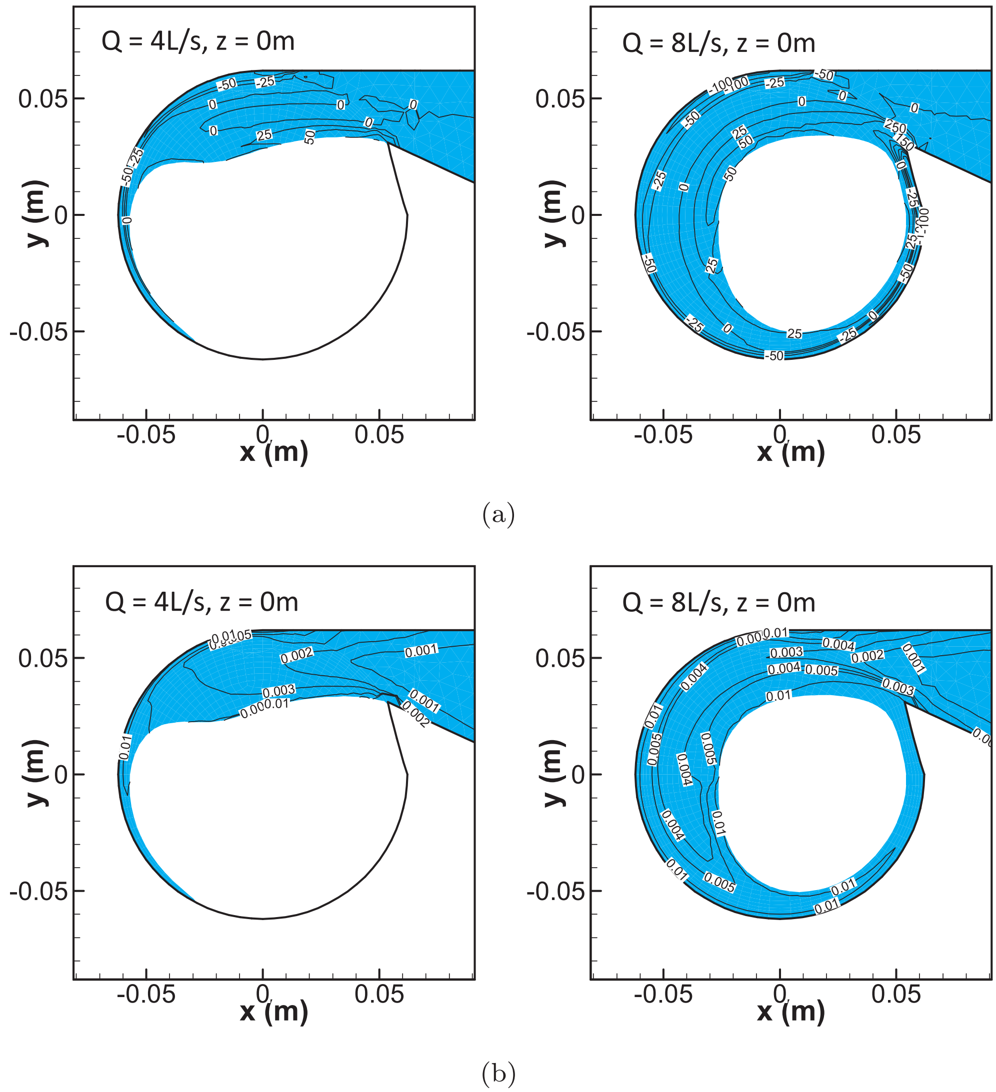

Fig. 13. (a) Predicted z-vorticity field and (b) total turbulent kinetic energy (TKE) field at $z = 0$m for $Q = 4$ L/s and 8 L/s.

model is developed for a stable tangential vortex intake and the numerical model results are validated against extensive experimental measurements of head-discharge relationship, air core size and the velocity field for a wide range of inflow conditions ($Q = 1$–10 L/s). The numerical model results revealed various interesting features of the vortex flow pattern in typical tangential intake. The inflow from the tapering inlet channel into the drop shaft is highly three-dimensional and can be divided into two regimes according to the free drainage condition at the junction. For a freely draining vortex flow, the streamwise horizontal x-velocity at the tapering channel-dropshaft junction varies linearly with elevation, while the vertical velocity variation is parabolic. The general vortex flow pattern is much more complex than the idealized symmetrical flow pattern normally assumed in 1D analytical models (Jain, 1984; Yu and Lee, 2009). Nevertheless the local tangential velocity of the swirling vortex flow in the drop shaft can be well-approximated by a Rankine-combined vortex model (i.e. forced vortex near the core and an outer free vortex in the main flow). Consistent with physical observations, the air core is not axisymmetric for a stable tangential vortex intake, but with a significant difference in the swirling flow depth (thickness) around the dropshaft. The minimum air core occurs at around the level of the tapering channel outlet and the air core size increases down the dropshaft. Unlike previous studies the variation of air core size with flow rate is successfully predicted for the first time. The present study offers comprehensive insights of tangential vortex intake flow, and provides a basis for the hydraulic design of such vortex intake structures. Videoclips of the stable tangential vortex intake flow can be found at https://youtu.be/Z-3Nk1_I_JE.

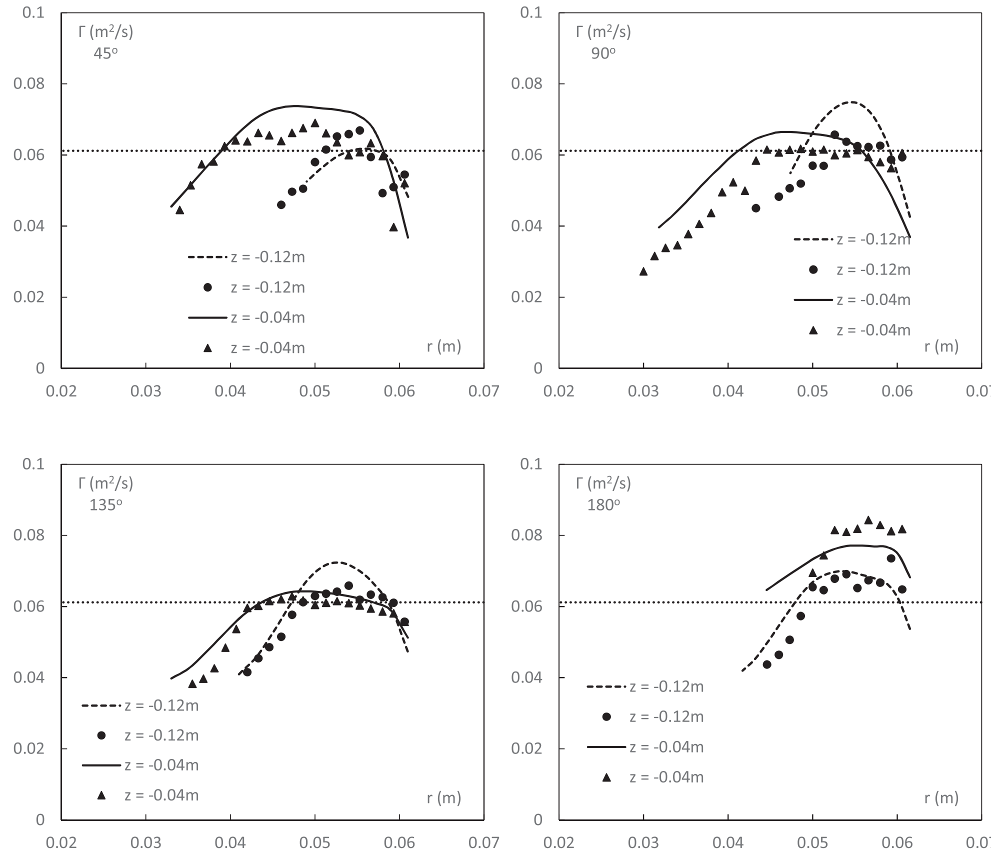

Fig. 14. Vortex circulation $\Gamma = u_\theta \times r$ (m^2/s) for $Q = 8$ L/s, lines: CFD, symbol: measurement, dotted line: predicted vortex circulation constant ($\Gamma_a = 0.61\ m^2/s$)

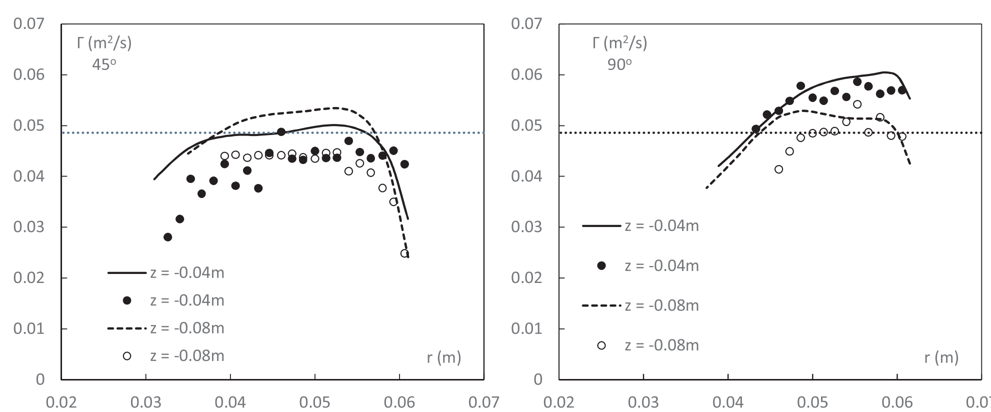

Fig. 15. Vortex circulation $\Gamma = u_\theta \times r$ (m^2/s) for $Q = 4$ L/s, lines: CFD, symbol: measurement, dotted line: predicted vortex circulation constant ($\Gamma_a = 0.48\ m^2/s$).

6. Application

The numerical modelling predictions of the air core size – an important design parameter – can be plotted on a dimensionless diagram that enables its application to many other designs. In Fig. 16 the normalized minimum air core area ratio λ_m is plotted against a dimensionless flow parameter $Q^* = (Q^2 e/gD^6)^{1/3}/(1-e/D)$. It is seen that all the experimental data and the present numerical model predictions fall on practically one line. An approximate fit of the collective numerical model predictions and data gives:

$$\lambda_m = 0.321Q^{*2} - 1.230Q^* + 1 \tag{8}$$

Eq. (8) can be used for an estimate of the air core size for the complex asymmetric tangential vortex intake flow.

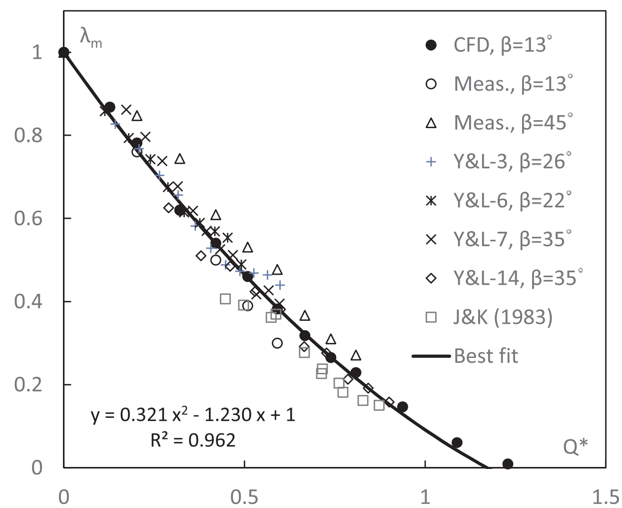

Fig. 16. Minimum air core area ratio λ_m against non-dimensional discharge $Q^* = (Q^2e/gD^6)^{1/3}/(1-e/D)$. Δ: Measured data of a similar design with $\beta = 45°$. Y &L: data in Yu and Lee (2009). J&K: data in Jain and Kennedy (1983).

Acknowledgment

This study was supported in part by a grant from the Hong Kong Research Grants Council (RGC HKU/HKUST 714309).

References

ANSYS Inc., 2013. ANSYS FLUENT 15.0 Theory Guide.

Binnie, A.M., Hookings, G.A., 1948. Laboratory experiments on whirlpools. Proc. R. Soc. Lond. Ser. A 194 (1038), 398–415.

Brooks, N.H., Blackmer, W.H., 1962. Vortex energy dissipator for San Diego ocean outfall – Laboratory investigation. Rep. No. KH-R-5. In: Keck, W.M., Laboratory of Hydraulics and Water Resources, California Institute of Technology, Pasadena, Calif.

Dantec Dynamics, 2006. BSA flow software. Publication No. 9040U5734, Tonsbakken 18, DK-2740 Skovlunde, Denmark.

Hirt, C.W., Nichols, B.D., 1981. Volume of fluid (VOF) method for the dynamics of free boundaries. J. Comput. Phys. 39 (1), 201–225.

Hite, J.E., Mih, W.C., 1994. Velocity of air-core vortices at hydraulic intakes. J. Hydraul. Eng. 120 (3), 284–297.

Jain, S.C., 1984. Tangential vortex-inlet. J. Hydraul. Eng. 110 (12), 1693–1699.

Jain, S.C., Kennedy, J.F., 1983. Vortex-Flow Drop Structures for the Milwaukee Metropolitan Sewerage District Inline Storage System. Report No. 264. Iowa Institute of Hydraulic Research, The University of Iowa, Iowa City, Iowa.

Lee, J.H.W., Chan, H.C., Yu, D.Y., Choi, D.K.W., 2005. Physical Hydraulic Model Tests for Hong Kong West Drainage Tunnel in Northern Hong Kong Island - Intake Structure. Final Report. Croucher Laboratory of Environmental Hydraulics, The University of Hong Kong.

Lee, J.H.W., Yu, D.Y., Choi, K.W., 2006. Physical Hydraulic Model Tests for Lai Chi Kok Transfer Scheme Intake Structure. Croucher Laboratory of Environmental Hydraulics, The University of Hong Kong.

Odgaard, A.J., 1986. Free-surface air core vortex. J. Hydraul. Eng. 112 (7), 610–620.

Plant, J., Crawford, D., 2016. Pushing the limits of tangential vortex intakes: is higher capacity and flow measurement possible in a smaller footprint? In: Proceedings of WEFTEC 2016. Water Environment Federation, New Orleans.

Qiao, Q.S., Lee, J.H.W., Lam, K.M., 2013. Steady vortex flow in tangential intake. In: Proceedings of 2013 IAHR World Congress. Chengdu, China.

Yu, D.Y., Lee, J.H.W., 2009. Hydraulics of tangential vortex intake for urban drainage. J. Hydraul. Eng. 135 (3), 164–174.

Zhao, C.H., Zhu, D., Sun, S.K., Liu, Z.P., 2006. Experimental study of flow in a vortex drop shaft. J. Hydraul. Eng. 132 (1), 61–68.